Anal. Chem. **2002,** *74,* 6323−6333

An Absorption-Based Surface Plasmon Resonance Sensor Applied to Sodium Ion Sensing Based on an Ion-Selective Optode Membrane

Kazuyoshi Kurihara,[†] Kaori Nakamura,[‡] Etsuko Hirayama,[‡] and Koji Suzuki*[,†,‡]

Kanagawa Academy of Science and Technology, 3-2-1 Sakado, Takatsu-ku, Kawasaki 213-0012, Japan, and Department of Applied Chemistry, Keio University, 3-14-1 Hiyoshi, Kohoku-ku, Yokohama 223-8522, Japan

A surface plasmon resonance (SPR) sodium ion sensor using an ion optode membrane film was experimentally and theoretically described based on an absorption-based SPR principle proposed in our previous article (Kurihara, K.; Suzuki, K. *Anal. Chem.* 2002, *74*, 696−701). The sodium ion concentrations from 10^{-6} to 10^{-1} have been successfully determined not only by the resonance angle diagnosis of the SPR curve but also by the minimum reflectance one. The ion optode film was plasticized poly(vinyl chloride) including a neutral sodium ionophore, a pH-sensitive cationic dye, and an anionic additive. Its optical absorption intensity changed with the sodium ion concentrations. The SPR ion sensor physically measured the complex refractive index caused by the absorption in the ion optode film. We have exhaustively investigated the experimental response behavior of the SPR curve relative to the sodium ion concentrations by comparison with numerically simulated SPR curves using a three-layer Fresnel equation including experimental values for the sodium ion optode membrane film. As predicted by the absorption-based SPR principle, the SPR curve behavior of the SPR ion sensors depended on two factors: one was the relation between the excitation frequency of the light source and the absorption maximum frequency in the ion optode film while the other was the gold metallic thickness in the Kretchmann configuration. The concept and practical theory of an absorption-based SPR sensor not only have been proved by the experimental results of the SPR sodium ion sensor but also have successfully allowed flexible ion sensing in an SPR sensor, which would be very difficult without the absorption mechanism in the ion optode film.

Surface plasmon resonance (SPR)[1] is a surface-sensitive analytical technique for (bio)chemical sensing[2] based on the detection of local changes in the refractive index (RI) within ~200-nm distance of a noble metal film surface. Recently, we proposed a new concept of absorption-based SPR[3] that detects changes in the complex RI due to the optical absorption. Conventional SPR monitors changes only in the usual RI, while absorption-based SPR measures changes in the RI imaginary part as well as the usual RI or the RI real part. Absorption-based SPR is founded on a more general principle than conventional SPR. One advantage of absorption-based SPR is that absorption analytical techniques can be introduced into the SPR method. At present, absorption-based SPR has great potential as an analytical tool but has not been fully developed in experiments. The practical theory of absorption-based SPR described in a previous paper[3] is very useful for understanding the responses of the SPR curve given by the reflectance versus the incident angle when optical absorption in the sensing layer of the SPR sensor system changes. The SPR curve behavior with increasing absorption is summarized in Figure 1, which shows that the minimum point behavior of the SPR curve is classified into six types. The concept and practical theory of absorption-based SPR will achieve a major breakthrough in SPR chemical and biochemical sensors.

As an analytical application of the absorption-based SPR, we now describe SPR ion sensors using a liquid membrane-based ion optode and simultaneously verify the absorption-based SPR principle using their experimental results. Actually, the practical theory of absorption-based SPR[3] has been developed to explain the SPR curve behavior of the SPR ion sensors in our previous reports.[4] Ion sensing is very difficult using the conventional SPR principle because the molecular weight of an ion is too low to cause a refractive index change due to the adsorption mechanism on the metal surface. The SPR ion sensors will be useful for multichannel SPR sensors[5−11] because the simultaneous detection of the target ions as well as biopolymers such as DNAs and

* Corresponding author. E-mail: suzuki@applc.keio.ac.jp.

[†] Kanagawa Academy of Science and Technology, 3-2-1 Sakado, Takatsu-ku, Kawasaki 213-0012, Japan.

[‡] Department of Applied Chemistry, Keio University, 3-14-1 Hiyoshi, Kohoku-ku, Yokohama 223-8522, Japan.

(1) Samble, J. R.; Bradbery, G. W.; Yang, F. *Contemp. Phys.* **1991**, *32*, 173−183.

(2) Homola, J.; Yee, S. S.; Gauglitz, G. *Sens. Actuators, B* **1999**, *54*, 3−15.

(3) Kurihara, K.; Suzuki, K. *Anal. Chem.* **2002**, *74*, 696−701.

(4) Kurihara, K.; Hirayama, E.; Nakamura, K.; Sasaki, S.; Citterio, D.; Suzuki. K. *Pittcon 2000* **2000**, 1323.

(5) Lee, H. J.; Goodrich, T. T.; Corn, R. M. *Anal. Chem.* **2001**, *73*, 5525−5531.

(6) Nelson, B. P.; Grimsrud, T. E.; Lies, M. R.; Goodman, R. M.; Corn, R. *Anal. Chem.* **2001**, *73*, 1−7.

(7) Brockman, J. M.; Nelson, B. P.; Corn, R. M. *Annu. Rev. Phys. Chem.* **2000**, *51*, 41−63.

(8) Johansen, K.; Arwin, H.; Lundstrom, I.; Liedberg, B. *Rev. Sci. Instrum.* **2000**, *71*, 3530−3538.

(9) Brockman, J. M.; Frutos, A. G.; Corn, R. M. *J. Am. Chem. Soc.* **1999**, *121*, 8044−8051.

(10) Berger, C. E. H.; Beumer, T. A. M.; Kooyman, R. P. H.; Greve, J. *Anal. Chem.* **1998**, *70*, 703−706.

10.1021/ac0203241 CCC: $22.00
Published on Web 11/15/2002

(a) SPR curve

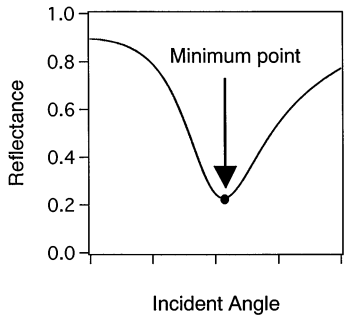

(b) Minimum point behavior of absorption-based SPR

		Relations between the excitation frequency, ω, and the absorption maximum frequency, ω_0.		
		$\omega > \omega_0$	$\omega = \omega_0$	$\omega < \omega_0$
Metallic Film	Thick			
	Thin			

Figure 1. Theoretical explanation of the absorption-based SPR curve behavior using (a) the minimum point of an SPR curve. (b) The SPR curve behavior with increasing absorption is classified into three times two types: three types according to the large, small, and equal relations between the excitation frequency, ω, and the absorption maximum frequency, ω_0; two types according to thin and thick metallic film.

proteins is practicable. The optode membrane consists of a pH-sensitive cationic absorption dye, a neutral ion-selective ionophore, and an anionic additive in the liquid membrane such as plasticized poly(vinyl chloride) (PVC). Its response mechanism was based on the ion-pair/ion-exchange principle, first described independently by Suzuki et al. and Simon et al.[12−18] The advantage of the liquid-based optode is flexibility in ion sensing, because there are a large number of ionophores selective for Li^+, Na^+, K^+, NH_4^+, Mg^{2+}, Ca^{2+}, Zn^{2+}, Ag^+, Hg^+, Pb^{2+}, Al^{3+}, and so on.[19] Simple replacement of an ionophore in the liquid membrane enables us to change the ion selectivity of the optodes. Also, replacement of the pH-sensitive dye allows us to control the dynamic range and the detection limit.

The present paper provides three important descriptions of the absorption-based SPR technique. First, the theory of the recently reported absorption-based SPR is correlated to the experimental results. The theory is further developed to account for the experimental conditions of the sensing layer that change the optical absorption spectra in the SPR sensor system. Second, a general method for ion sensing in SPR sensors has been successfully established. Ion sensing is very difficult using the conventional SPR principle[20] but is much easier with the absorption-based SPR principle. A sodium-selective SPR ion sensor is demonstrated as an SPR ion sensor based on an ion-selective optode membrane whose selectivity can be easily controlled by the replacement of the neutral ionophore in the membrane. Third, it is clearly demonstrated that a cooperative combination of the concept and the practical theory of absorption-based SPR is a driving force in developing a new SPR biochemical and chemical sensor. The concept provides scientific motivation to introduce absorption analytical techniques into the SPR method, while the practical theory resolves technical problems in realizing a new SPR biochemical and chemical sensor. In addition, the concept and practical theory of absorption-based SPR will be useful for improving some conventional SPR sensing methods such as electrochemical SPR[21−23] and colloidal Au nanoparticle-enhanced SPR[24] that are closely related to the absorption-based SPR principle. Therefore, the present paper gives practical descriptions of the absorption-based SPR technique while the previous paper provided only a theoretical description.

THEORY

Operation Principle of Ion-Selective Optodes. The sensing layer is an ion-selective optode membrane based on a plasticized PVC membrane. Its response mechanism is explained by the ion-pair extraction/ion exchange principles.[12−14] In the case where a neutral ionophore, S, selective for the target ion, i^+, a deprotonated cationic dye, D, and a lipophilic anionic additive, R^- are incorporated, the response mechanism is given by the following chemical equilibrium:

$$i_w^+ + S_o + DH^+R_o^- \leftrightarrow Si^+R_o^- + D_o + H_w^+ \qquad (1)$$

where H^+ is the hydrogen ion; DH^+R^- is the ion pair of the protonated dye and an additive, and Si^+R^- is the ion pair of the ion−ionophore complex and an additive. Subscripts o and w mean that the chemical species is in the organic phase and the water phase, respectively. The hydrogen ion is exchanged for the target ion in the water phases when the target ion complexes with the ionophore in the organic phase. Simultaneously, the dye in the organic phase transfers from the protonated form, DH^+, to the neutral form, D, with the result that its spectrum of absorption or fluorescence changes. According to the law of mass action, the chemical equilibrium of eq 1 gives the following equation:

(11) Jordan, C. E.; Frutos, A. G.; Thiel, A. J.; Corn, R. M. *Anal. Chem.* **1997**, *69*, 4939−4947.
(12) Suzuki, K., Ohzora, H.; Tohda, K.; Miyazaki, K.; Watanabe, K.; Inoue, H.; Shirai, T. *Anal. Chim. Acta* **1990**, *237*, 155−164.
(13) Watanabe, K.; Nakagawa, E.; Yamada, H.; Hisamoto, H.; Suzuki, K. *Anal. Chem.* **1993**, *65*, 2704−2710.
(14) Hisamoto, H.; Watanabe, K.; Nakagawa, E.; Siswanta, D.; Shichi, Y.; Suzuki, K. *Anal. Chim. Acta* **1994**, *299*, 179−187.
(15) Morf, W. E.; Seiler, K.; Rusterholz, B.; Simon, W. *Anal. Chem.* **1990**, *62*, 738−742.
(16) Seiler, K.; Simon, W. *Anal. Chim. Acta* **1992**, *266*, 73−87.
(17) Bakker, E.; Simon, W. *Anal. Chem.* **1992**, *64*, 1805−1812.
(18) Bakker, E.; Buhlmann, P.; Pretsch, E. *Chem. Rev.* **1997**, *97*, 3083−3132.
(19) Buhlmann, P.; Pretsch, E.; Bakker, E. *Chem. Rev.* **1998**, *98*, 1593−1687.
(20) Ozawa, T.; Kakuta, M.; Sugawara, M.; Umezawa, Y. *Anal. Chem.* **1997**, *69*, 3081−3085.
(21) Iwasaki, Y.; Tobita, T.; Kurihara, K.; Horiuchi, T.; Suzuki, K.; Niwa, O. *Biosens. Bioelectron.* **2002**, *17*, 783−788.
(22) Iwasaki, Y.; Horiuchi, T.; Niwa, O. *Anal. Chem.* **2001**, *73*, 1595−1598.
(23) Brennan, C. B.; Sun, L.; Weber S. G. *Sens. Actuators, B* **2001**, *72*, 1−10.
(24) He, L.; Musick, M. D.; Nicewarner, S. R.; Salinas, F. G.; Benkovic, S. J.; Natan, M. J.; Keating, C. D. *J. Am. Chem. Soc.* **2000**, *122*, 9071−9077.

$$K_{exch} = \frac{[Si^+R_o^-][D_o][H_w^+]}{[i_w^+][S_o][DH^+R_o^-]} \quad (2)$$

where the brackets represent the concentration of the chemical species and K_{exch} is the equilibrium constant. The target ion concentration can be described with the experimental conditions of the total ionphore concentrations, $[S_{tot}]$, the total cationic dye concentration, $[D_{tot}]$, and the total anionic additive, $[R^-]$, as follows:

$$[i_w^+] = \frac{[H_w^+]}{K_{exch}} \frac{\alpha}{1-\alpha} \frac{[R_{tot}] - (1-\alpha)[D_{tot}]}{[S_{tot}] - [R_{tot}] + (1-\alpha)[D_{tot}]} \quad (3)$$

with

$$\alpha = [D_o]/[D_{tot}] \quad (4)$$

where α is the relative portion of the deprotonated cationic dye. Equation 3 is a quadratic equation for α. Under a special condition given by

$$[S_{tot}] = (1 + \Delta_S)[D_{tot}] \quad (5)$$

$$[R_{tot}] = (1 + \Delta_R)[D_{tot}] \quad (6)$$

with

$$1 \gg \Delta_S, \Delta_R \quad (7)$$

an approximate value of α is given by

$$\alpha \cong \alpha_0 + \alpha_1\left(1 + \sqrt{\frac{[H_w^+]}{K_{exch}[i_w^+]}}\right)^{-1} \quad (8)$$

with

$$\alpha_0 = -\Delta_R/2 \quad (9)$$

and

$$\alpha_1 = 1 + \Delta_S \quad (10)$$

Equation 8 is a practical equation to explain the experimental response of the ion optode membrane. When α as a function of $[i_w^+]$ under a certain pH condition is experimentally obtained, eq 8 can be used as a fitting equation with parameters of α_0, α_1, and K_{exch}.

In absorption spectroscopy, when only the dye of the neutral form contributes to absorption of light at a certain wavelength, the molar concentration of absorption oscillators, [Ab], is given by

$$[Ab] = \alpha[D_{tot}] \quad (11)$$

According to Lambert−Beer's law, the absorbance, $A(\omega)$, at a frequency, ω, is described by

$$A(\omega) = \epsilon^{Ab}(\omega)[Ab](l/100) \quad (12)$$

where $\epsilon^{Ab}(\omega)$ is the molar decadic absorption coefficient at the frequency, ω and l is the length of the absorption layer in metric units. Equations 11 and 12 show that the absorbance response of the ion optode membrane film, $A(\omega)$, with a thickness of l is described by

$$A(\omega) = A_0(\omega)\alpha \quad (13)$$

with

$$A_0(\omega) = \epsilon^{Ab}(\omega)[D_{tot}](l/100) \quad (14)$$

Absorbance spectra of the ion optode membrane film, $A(\omega)$, can be tied to the relative portion of the deprotonated cationic dye, α, in eqs 8−13. In particular, the term $A(\omega = \omega_0)$ that indicates the absorbance when the incident frequency, ω, equals the frequency at the absorption maximum, ω_0, plays an important role in describing the experimental dielectric constant of the ion optode membrane as you can see below.

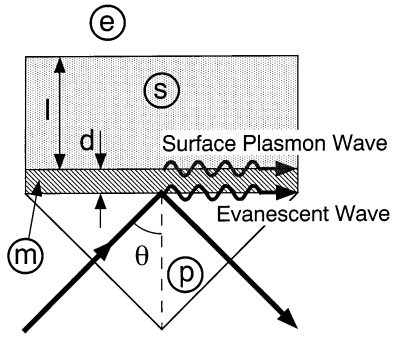

Figure 2. Kretchmann configuration of a prism−metal film−sensing layer−environment interface. The glass prism, the metallic film, the sensing layer, and the environment are labeled p, m, s, and e, respectively. In our case, the sensing layer is a sodium ion-selective optode membrane film that changes its absorption spectrum due to the sodium ion concentration. θ is the incident angle while d and l are the thicknesses of the metallic film and sensing layer, respectively. The surface plasmon wave is resonantly excited by the evanescent wave generated by the incident light when both the wavenumbers are matched.

Theory of an Absorption-Based SPR Ion Sensor. As shown in Figure 2, an SPR ion-sensor is a four-layer system that consists of a prism−metal−sensing layer−environment interface under a Kretschmann attenuated total reflection (ATR) configuration. However, the three-layer system without the environment is valid for theoretically and numerically describing SPR responses when the sensing layer is so thick that the environmental effect can be ignored. In Figure 2, a glass prism, a metallic film, a sensing layer, and the external environment are labeled p, m, s, and e, respectively. When the P-polarized light is incident at an angle θ, the reflectance R of the light is given by the three-layer Fresnel equation of P-polarization as follows[3]:

$$R = \left|\frac{r_{pm} + r_{ms}\exp(2ik_{mz}d)}{1 + r_{pm}r_{ms}\exp(2ik_{mz}d)}\right|^2 \quad (15)$$

with

$$r_{pm} = (\epsilon_p k_{mz} - \epsilon_m k_{pz})/(\epsilon_p k_{mz} + \epsilon_m k_{pz}) \quad (16)$$

$$r_{ms} = (\epsilon_m k_{sz} - \epsilon_s k_{mz})/(\epsilon_m k_{sz} + \epsilon_s k_{mz}) \quad (17)$$

and

$$k_{jz} = (\epsilon_j(\omega^2/c^2) - k_x^2)^{1/2} \quad \text{for} \quad j = \text{p, m, s} \quad (18)$$

$$k_x = \sqrt{\epsilon_p}\frac{\omega}{c}\sin\theta \quad (19)$$

where r_{pm} and r_{ms} are the amplitude reflectance given by the Fresnel formulas of P-polarization for the prism−metal and metal−sensing layer interfaces, respectively; ϵ_j and k_{jz} are the dielectric constant and the wave vector component perpendicular to the interface in medium j; k_x is the component of the incident wave vector parallel to the interface; d is the thickness of the metallic film; ω is the angular frequency of the incident light; and c is the velocity of light.

The optical characteristics of the three layers can be expressed in the dielectric constant. The dielectric constant of the prism layer ϵ_p is described by

$$\epsilon_p = n_p^2 \quad (20)$$

where n_p is the refractive index of the prism. The dielectric constant of the metal layer ϵ_m is obtained by assuming a Drude model so that

$$\epsilon_m = \epsilon_m^\infty - \omega_p^2/\omega(\omega + i\omega_\tau) \quad (21)$$

with

$$\omega = 2\pi c/\lambda \quad (22)$$

where ω and λ are the frequency and the wavelength of incident light, respectively; c is the light velocity; ω_p and ω_τ are the plasma frequency and the damping frequency, respectively; and ϵ_m^∞ is the background dielectric constant of the metal layer at a frequency of infinity. According to the curve fitting of reliable data in the literature,[25] gold metal has $\epsilon_m^\infty = 9.75$, $\omega_p = 1.36 \times 10^{16}$ rad/s, and $\omega_\tau = 1.45 \times 10^{14}$ rad/s in the range of 600−900 nm. The dielectric constant ϵ_s of the sensing layer that consists of N absorption oscillators per unit volume is obtained by assuming a Lorentz model as follows,

$$\epsilon_s(\omega) = \epsilon_s^\infty + N\frac{e^2}{m_e\epsilon_0}\frac{f}{\omega_0^2 - \omega^2 - i\omega\gamma} \quad (23)$$

with

$$\omega_0 = 2\pi c/\lambda_{max} \quad (24)$$

$$\gamma = 2\pi c(\lambda_{1/2}/\lambda_{max}^2) \quad (25)$$

$$\epsilon_0 = 10^7/4\pi c^2 \quad (26)$$

and

$$N = 10^3 N_A[\text{Ab}] \quad (27)$$

where e is the elementary electric charge; m_e is the mass of an electron; ϵ_0 is the permittivity of a vacuum; ω_0 and γ are the absorption frequency and the damping frequency, respectively; λ_{max} and $\lambda_{1/2}$ are the absorption maximum wavelength and the full width wavelength at half-maximum of the absorption spectrum, respectively; f is the oscillator strength, which is related to the molar extinction coefficient; ϵ_s^∞ is the background dielectric constant of the sensing layer; N_A is Avogadro's constant; and [Ab] is the above-mentioned molar concentration of the absorption oscillators given in eq 11.

In the case where the absorbance spectrum of the sensing layer is obtained, the dielectric constant ϵ_s in eqs 23−27 can be rewritten in the absorbance, $A(\omega_0)$, at the maximum absorption wavelength. When the real part, n_s, and the imaginary part, κ_s, of the refractive index in the sensing layer are defined by

$$n_s + i\kappa_s \equiv \sqrt{\epsilon_s} \quad (28)$$

the approximation of eq 23 under the condition of [Ab] ≪ 1 gives a useful expression for the RI imaginary part as follows:

$$\kappa_s(\omega) \cong [\text{Ab}]\frac{10^3 N_A e^2 f}{2\sqrt{\epsilon_s^\infty} m_e \epsilon_0}\frac{\omega\gamma}{(\omega_0^2 - \omega^2)^2 + (\omega\gamma)^2} \quad (29)$$

In particular, when $\omega = \omega_0$, eq 29 is transformed to

$$\kappa_s(\omega_0) \cong [\text{Ab}]\frac{10^3 N_A e^2 f}{2\sqrt{\epsilon_s^\infty} m_e \epsilon_0}\frac{1}{\omega_0\gamma} \quad (30)$$

so that the dielectric constant ϵ_s in the sensing layer can be described using eq 30 by

$$\epsilon_s(\omega) = \epsilon_s^\infty + \frac{2\sqrt{\epsilon_s^\infty}\kappa_s(\omega_0)\omega_0\gamma}{\omega_0^2 - \omega^2 - i\omega\gamma} \quad (31)$$

On the other hand, the optics theory indicates that the absorption coefficient, a, is given by

$$a = 2\kappa_s\omega/c \quad (32)$$

while the absorbance, A, is given by

(25) Innes, R. A.; Sambles, J. R. *J. Phys. F: Met. Phys.* **1987**, *17*, 277−287.

$$A = al/\ln 10 \tag{33}$$

where l is the above-mentioned length of the absorption layer. Combination of eqs 32 and 33 yields

$$A(\omega) = (2l\kappa_s(\omega)\omega)/(c \ln 10) \tag{34}$$

Finally, substitution of eq 34 at $\omega = \omega_0$ into eq 31 gives an experimentally useful equation for the dielectric constant ϵ_s in eq 23 as follows:

$$\epsilon_s(\omega) = \epsilon_s^{\infty} + \frac{A(\omega_0)}{l} \frac{\sqrt{\epsilon_s^{\infty}} c\gamma \ln 10}{\omega_0^2 - \omega^2 - i\omega\gamma} \tag{35}$$

Equation 35 indicates that the dielectric constant ϵ_s in the sensing layer can be expressed by the following five experimental values: the absorption maximum frequency, ω_0, the absorption damping frequency, γ, the absorbance of the sensing layer at the absorption maximum frequency, $A(\omega_0)$, the thickness of the sensing layer, l, and the background dielectric constant of the sensing layer, ϵ_s^{∞}. The absorbance measurement of the ion optode membrane determines the values of ω_0, γ and $A(\omega_0)$ due to eqs 24, 25, and 13 with eq 8, respectively. Thickness measurements using atomic force microscopy can experimentally determine the value of l. The value of ϵ_s^{∞} is experimentally obtained by squaring the usual RI of the ion optode membrane measured by the refractometer. Numerical simulations taking in the experimental parameters of the ion optode membrane can be done with eq 35 added to eqs 15−22.

EXPERIMENTAL SECTION

Reagent. Sodium ionophore (DD16C5), tetrakis[3,5-bis-(trisfluoromethyl)phenyl]borate sodium salt dihydrate (TFPB) used as a anionic additive and 2-nitrophenyl octyl ether (NPOE) used as a plasticizer were purchased from Dojindo Laboratory (Kumamoto, Japan). Poly(vinyl chloride) (PVC; high molecular weight type) was purchased from Sigma (St. Louis, MO). Lipophilic cationic dye (KD-M11) was synthesized according to our report.[26] The chemical structures of DD16C5, KD-M11, TFPB, and NPOE are shown in Figure 3.

Standard Solutions. The buffer solution was 0.05 M tris-(hydroxymethyl)aminomethane (Tris)-HCl buffer (pH 7). The standard solutions of Na^+ (Na^+ test solutions) were 10^{-6}−10^{-1} M NaCl in the buffer solution. The test acid and base solutions were HCl (pH 2) and NaOH (pH 11) aqueous solutions.

Membrane Cocktail of Sodium Ion-Selective Optode. The membrane cocktail was prepared for forming a thin film by the spin-coating method. The membrane cocktail of the sodium ion-selective optode contained DD16C5 (4.06 μmol), KD-M11 (4.06 μmol), TFPB (4.06 μmol), NPOE (80 mg), and PVC (40 mg), which were dissolved in tetrahydrofuran (THF).

Preparation of SPR Chips for Sodium Ion Sensing. The glass plate for the SPR chips was a high-refractive-index glass plate (20 × 51 × 1 mm) made of SFL6 glass (Ohara, Kanagawa, Japan)

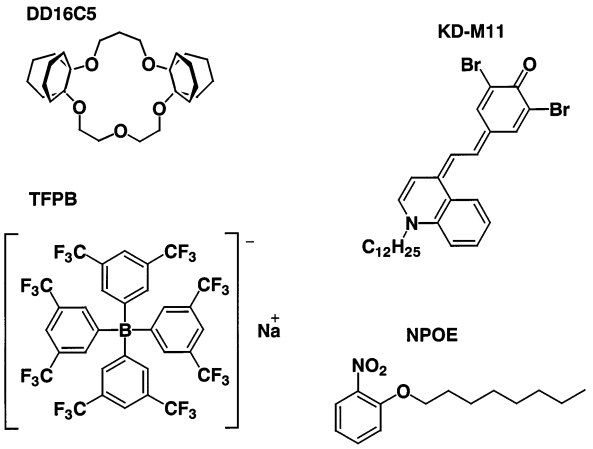

Figure 3. Chemical structures of sodium ion-selective neutral ionophore of DD16C5, lipophilic cationic dye of KD-M11, anionic additive of TFPB, and plasticizer of NPOE.

with a refractive index of ∼1.80 from 600 to 700 nm. A gold metallic film with two different thicknesses of about 28 and 50 nm was coated on the central region (20 × 19 mm) of the glass plate by the sputtering method. The gold metallic thickness was experimentally checked within an accuracy of 5 nm using an atomic force microscope (Nanopics 1000, Seiko Instruments, Inc., Tokyo, Japan). A titanium metallic film of a few nanometers thickness was also coated between the gold metallic film and the glass plate for good adhesion. The membrane cocktail for the sodium ion-selective optode was dropped on the gold metallic film-coated glass plate that was fixed on a spin coater (Mikasa, Tokyo, Japan), which was rotated for 5 s at 4000 rpm to form a thin film of the optode membrane. The spin-coated ion optode membrane film was dried under vacuum to evaporate the THF solution in the optode membrane. SPR chips were ready for the SPR ion-sensing measurements after immersion into HCl aqueous solution (pH 2) for 10 min and then into Tris buffer solution (pH 7) for 5 h.

SPR Measurements. All the SPR measurements were performed using an SPR sensor system (DKK Co., Tokyo, Japan) that detected a reflected angular spectrum of the convergent monochromatic light under a Kretchmann ATR configuration. SPR curves were obtained by dividing a P-polarized angular spectrum by an S-polarized one to compensate for the inhomogeneous distribution of the convergent light intensity. For our applications, optical elements in the SPR sensor system such as the prism and the light-emitting diode (LED) were replaced. The replaced prism as well as the glass plate for SPR chips was made of a high-refractive-index glass, SFL6 glass, with a refractive index of 1.80 because the SPR phenomenon requires that the prism have a much larger refractive index than the ion-selective optode membrane with a typical refractive index of 1.52. An index-matching oil with a refractive index of 1.780 (R.P. Cargille Laboratories, Inc.) was used between the prism and the SPR chip in order to eliminate the unwanted reflection. In our SPR system, two kinds of LEDs were available for the investigation of SPR curve behavior that depends on the excitation wavelength. The LEDs have a Lorentz resonance curve spectrum that peaks at 637 and 656 nm with a full width at half-maxumum (fwhm) of 20 and 19 nm, respectively. In SPR measurements, broadband neutral density filters to reduce the light intensity were often used for adjusting the light intensity

(26) Hisamoto, H.; Tohma, H.; Yamada, T.; Yamauchi, K.; Siswanta, D.; Yoshioka, N.; Suzuki, K. *Anal. Chim. Acta* **1998**, *373*, 271−289.

of the LED to the dynamic range of the charge-coupled imaging device (CCD) in the SPR system.

Angular Resolution and Accuracy of SPR Measurements. The angular resolution of the SPR measurements was experimentally estimated using simple slits with widths of 2, 1, and 0.5 mm that were made of paper. The slits were used for converting the broad beam of the convergent incident light into a narrow beam. The narrow beam gave a narrow width of the reflected angular spectrum, which reaches the angular resolution of the SPR measurements when the width of the slit approaches zero. The typical angular resolution was determined to be ~0.6° at the center of the observed area. On the other hand, the angular accuracy in the SPR measurements is described using two aspects of the scale and the value. The angular accuracy of the scale was calibrated within an accuracy of 10% by measuring the displacement of the SPR angle in the CCD image due to the rotation of the goniometer in the SPR system by a certain angle. The angular accuracy of the value was estimated to be low, ~3°, because the prism was roughly set on the goniometer during each measurement. Nevertheless, the low angular accuracy of the value was not a critical problem in an SPR chemical sensor that measures not the value of the angle but a change in the angle.

Absorption Spectrophotometry of the Ion Optode Membrane Film. To experimentally determine three values of the absorption frequency, ω_0, the damping frequency, γ, and the absorbance at the absorption frequency, $A(\omega_0)$, in eq 35, the absorption spectrophotometery of the ion optode membrane film was determined using a spectrophotometer (U-2000, Hitachi, Tokyo, Japan). The ion optode membrane film for absorption spectrophotometry was obtained by dropping the optode membrane cocktail on a transparent plastic sheet and then spin-coating it for 5 s at 4000 rpm. The membrane film was cut into a 10 × 50 mm rectangle and placed in the quartz cell of the spectrophotometer. The ion optode membrane film was available for absorption measurements after the membrane film was immersed into HCl aqueous solution (pH 2) for 10 min and then into Tris buffer solution (pH 7) for 5 h. Absorption spectra of the ion optode membrane film were obtained at various Na^+ concentrations with due caution against waiting much longer than the response time, typically 10 min, which depends on the concentrations.

Thickness Measurements of the Ion Optode Film in the SPR Chips. To experimentally determine the length of the absorption layer, l, in eq 35, a thickness measurement of the optode membrane film that was spin-coated on the gold-coated glass plate was performed using the above-mentioned atomic force microscope. A narrow groove was scratched in the optode membrane film on the substrate using a small screwdriver. The depth of the groove corresponds well with the thickness of the absorption layer. We carefully carried out the thickness measurement several times, with the result that the thickness of the optode membrane film was $l = 1.0 \pm 0.3\ \mu$m.

Refractive Index Measurements of the Ion Optode Membrane. To experimentally determine the value of the background dielectric constant, ϵ_s^∞, in eq 35, refractive index measurements of the ion optode membrane were carried out using a refractometer (RX-5000α, Atago Co., Tokyo, Japan), which measures the refractive index at the sodium D line, 589.3 nm. The square of the measured refractive index gives the background dielectric constant, ϵ_s^∞. A membrane cocktail of the sodium ion-selective optode without the cationic dye (KD-M11) was used to eliminate a variation in the usual refractive index due to the absorption effect of the cationic dye. The membrane cocktail was dropped on the measurement cell in the refractometer and left alone for more than 6 h at room temperature to evaporate the THF solution in the optode membrane. The refractive index of the ion optode membrane "without the cationic dye" was 1.52 RI units, which was only approximate but was appropriate as an experimental value of the background refractive index of the ion optode membrane "with the cationic dye". Thus, we obtained an experimental value of the background dielectric constant, $\epsilon_s^\infty = 2.31$.

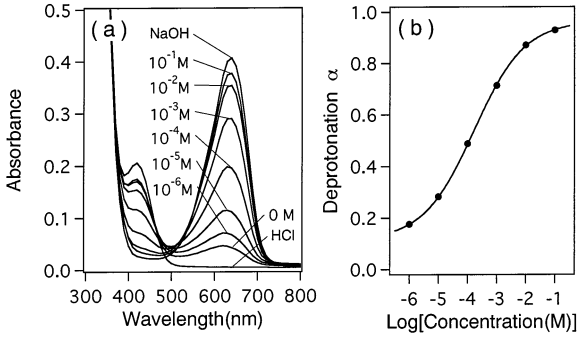

Figure 4. Optical response of sodium ion-selective optode membrane film to sodium ion solutions. (a) Absorbance spectra of the optode membrane film at various sodium ion concentrations of 0, 10^{-6}, 10^{-5}, 10^{-4}, 10^{-3}, 10^{-2}, and 10^{-1} M in the pH 7 buffer and in two aqueous solutions of HCl (pH 2) and NaOH (pH 11). (b) The relative portion, α, of deprotonated dye in the optode membrane related to various sodium ion concentrations of 10^{-6}–10^{-1} M when the deprotonation is assumed to be α = 1 in the NaOH solution. The response curve was obtained by fitting the data to eq 8.

RESULTS AND DISCUSSION

Determination of the Dielectric Constant of the Ion Optode Film. Experimental determination of the dielectric constant of the ion optode film given by eq 35 enables us to do numerical simulations of SPR curves, which are useful for mutual checks between theoretical and experimental results. There are five experimental parameters, ϵ_s^∞, l, ω_0, γ, and $A(\omega_0)$, in eq 35, which were experimentally determined by the refractive index measurement, the thickness measurement, and the absorbance measurement. As described in the Experimental Section, the background dielectric constant, $\epsilon_s^\infty = 2.31$, and the length of the absorption layer, $l = 1.0 \times 10^{-6}$ m, were experimentally obtained. On the other hand, the experimental values of three parameters, ω_0, γ, and $A(\omega_0)$, were obtained by the absorbance measurement. Figure 4a shows the absorbance spectra of the sodium ion-selective optode film at various sodium ion concentrations from 0 to 10^{-1} M in the pH 7 buffer, and two aqueous solutions of HCl and NaOH. All the cationic dyes in the optode membrane were protonated in HCl solution but deprotonated in NaOH solution, so that the relative portion of deprotonated cationic dye, α, is described as α = 0 in HCl solution and α = 1 in NaOH solution. In Figure 4a, the absorption maximum shifts from 635 nm at 10^{-1} M to 621 nm at 10^{-6} M; but in numerical simulation, we used an absorption maximum of $\lambda_{max} = 631 \times 10^{-9}$ m, obtained as the average of the absorption maximums of available concentrations from 10^{-1} to 10^{-6} M in Figure 4a. The fwhm of the absorption

Table 1. Experimental Values for the Dielectric Constant, Eq 35, in the Sodium Ion-Sensitive Layer

background dielectric constant	$\epsilon_s^{\infty} = 2.31$
thickness of the sensing layer	$l = 1.0 \times 10^{-6}$ (m)
absorption maximum frequency	$\omega_0 = 2.99 \times 10^{15}$ (s^{-1})
damping frequency of the absorption	$\gamma = 5.20 \times 10^{14}$ (s^{-1})
absorbance as a function of ion concentrations	$A(\omega_0) = 0.0471 + 0.344/(1 + \sqrt{1.68 \times 10^{-4}/[i^+]})$

spectrum was $\lambda_{1/2} = 110 \times 10^{-9}$ m for numerical simulation. The absorption frequency, $\omega_0 = 2.99 \times 10^{15}$ s^{-1}, and the damping frequency, $\gamma = 5.20 \times 10^{14}$ s^{-1}, were then obtained using eqs 24 and 25. Figure 4b shows the deprotonation of the cationic dye as a function of the sodium ion concentrations, where the closed circles were obtained by dividing each absorbance by the absorbance of NaOH at the absorption maximum. The solid line was obtained by fitting the closed circles to eq 8 with three unknown parameters, α_0, α_1, and K_{exch}, under the condition of $[H_w^+] = 10^{-7}$. The numerical fitting procedure determined $\alpha_0 = 0.116$, $\alpha_1 = 0.848$, and $K_{exch} = 5.96 \times 10^{-4}$. On the other hand, the absorbance of NaOH at the absorption maximum in Figure 4a gave $A_0(\omega_0) = 4.06$ in eq 13. Finally, $A(\omega_0)$ was given by

$$A(\omega_0) = 0.0471 + \frac{0.344}{1 + \sqrt{1.68 \times 10^{-4}/[i_w^+]}} \qquad (36)$$

Table 1 shows five experimental values of the parameters, ϵ_s^{∞}, l, ω_0, γ, and $A(\omega_0)$, describing the dielectric constant of the ion optode film in eq 35 for numerical simulations.

It is worth describing the meaning of the fitting of data in Figure 4b using eq 8, which is, to our knowledge, first described in the present paper. Equation 8 is practically useful as a fitting equation and also is based on the attractive hypothesis that not all the sensing components in the ion optode membrane are involved in the response mechanism described by the ion-pair extraction/ion-exchange principles. Although our preparation conditions for the sodium ion-selective optode membrane theoretically ought to give $\Delta_S = \Delta_R = 0$ according to eqs 5 and 6, the experimental results gave $\Delta_S = -0.232$ and $\Delta_R = -0.152$ through the fitting procedure. In addition, the preparation conditions cannot explain the difference in the absorbance spectrum between 0 M concentration and HCl solution in Figure 4a without the hypothesis of the existence of sensing components not involved in the response mechanism. It is noted that the hypothesis cannot be attributed to the activity coefficient. In the present stage of our experiments, we cannot explain why some sensing components are not involved in the response mechanism, but the hypothesis is intensely practical for deriving the fitting equation, eq 8, that successfully combines experimental results with the theoretical equations.

SPR Curve Behavior of Absorption-Based SPR Sodium Ion Sensors and Its Comparison with Numerical Simulation. In experiments on absorption-based SPR sodium ion sensors, the SPR curve response to sodium ion concentrations of 10^{-6}–10^{-1} M was observed under three kinds of conditions: excitation wavelengths of 637, 656, and 637 nm with metallic film thicknesses of 50, 50, and 28 nm in part a of Figure 5, Figure 6 and, Figure 7, respectively. When the practical theory in Figure 1b is considered, the three conditions are described as $\omega = \omega_0 - 0.05\gamma$ with a thick metallic film for Figure 5, $\omega = \omega_0 - 0.22\gamma$ with a thin metallic film for Figure 6, and $\omega = \omega_0 - 0.05\gamma$ with a thin metallic film for Figure 7. Here, ω is the excitation frequency in eq 22, ω_0 is the absorption maximum frequency in eq 24, and γ is the absorption damping frequency in eq 25. Part b of Figures 5–7 is the sodium ion concentration dependence of the minimum reflectance, R_{min}, and its incident angle, θ_{min}, known as the resonance angle, which were determined using the asymmetric SPR curve-fitting equation[27] we have recently proposed as follows:

$$R(\theta) = A\left(1 - \frac{B + C(X - \theta)}{(\theta - D)^2 + E^2}\right) \qquad (37)$$

where θ is the incident angle, $R(\theta)$ is the reflectance as a function of the incident angle, and A, B, C, D, and E are parameters for fitting an experimental SPR curve. Equation 37 contains the reflectance minimum, R_{min}, and the resonance angle, θ_{min}, as follows:

$$R_{min} = A\left(1 - \frac{B + \sqrt{B^2 + C^2E^2}}{2E^2}\right) \qquad (38)$$

and

$$\theta_{min} = D + \frac{-B + \sqrt{B^2 + C^2E^2}}{C} \qquad (39)$$

A fitting equation of the S-type curve in part b of Figures 5–7 was obtained by a simple assumption that both R_{min} and θ_{min} change in proportion to the relative portion of the deprotonated cationic dye, α, in eq 8. With this assumption, the fitting equation, $f([i_w^+])$, as a function of target ion concentration, $[i_w^+]$, in the water phase is given by

$$f([i_w^+]) = c_0 + c_1\left(1 + \frac{c_2}{\sqrt{[i_w^+]}}\right)^{-1} \qquad (40)$$

where c_0, c_1, and c_2 are fitting parameters. Part c of Figures 5–7 is a numerical simulation of experimental SPR curves in part a of Figures 5–7, respectively, using a set of the three-layer Fresnel equation regarding P-polarization, which consists of eqs 15–22, 24, 25, and 35 with the experimental values in Table 1. Part d of Figures 5–7 is also a numerical simulation that includes spectral broadening of the light source in part c of Figures 5–7, respectively, so that agreement in SPR curve behavior between experimental results and numerical simulations has been improved much more. Only a slight improvement in the agreement was obtained by a further simulation that included the experimental angular resolution of 0.6° in the SPR measurement.

In Figures 5 and 6, the metallic thickness of 50 nm applies to the thick case in Figure 1. A comparison of the SPR curve behavior

(27) Kurihara, K.; Nakamura, K.; Suzuki, K. *Sens. Actuators, B* **2002**, *86*, 49–57.

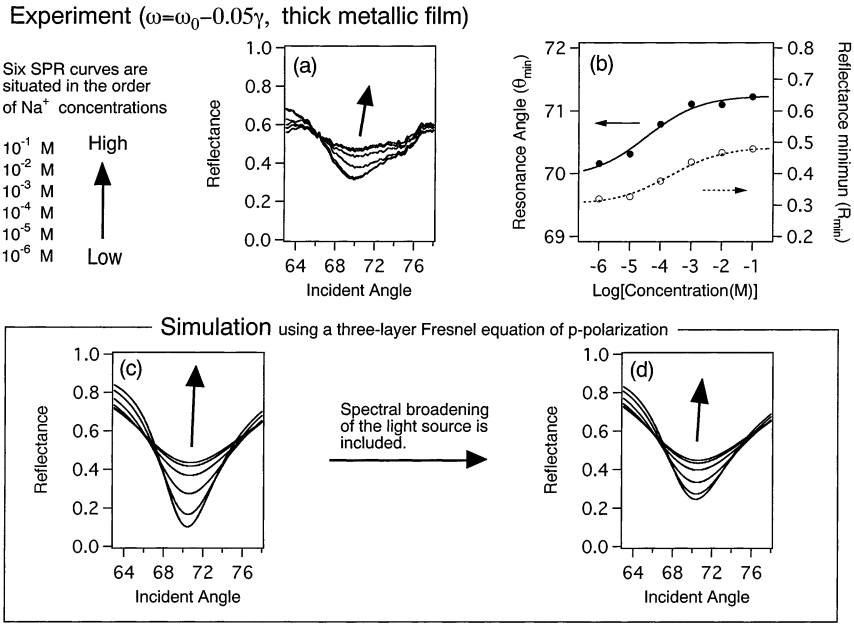

Figure 5. SPR curve response of the SPR sodium ion sensor with a thick metallic thickness of 50 nm under an excitation condition of $\omega = \omega_0 - 0.05\gamma$, where ω, ω_0. and γ are the excitation frequency, the absorption maximum frequency, and the absorption damping frequency related to the fwhm of absorption spectrum. (a) SPR curves respond to sodium ion concentrations from 10^{-6} to 10^{-1} M. They are situated in the direction of the arrow as the sodium ion concentrations changes from 10^{-6} to 10^{-1} M. (b) Dependence of the resonance angle and the reflectance minimum on the sodium ion concentrations. Closed and open circles are data on the resonance angle and the reflectance minimum, respectively, of the SPR curve. They are obtained by fitting the experimental SPR curves in part a to the asymmetric SPR curve-fitting eq 37. Also, the solid and broken lines are obtained by fitting data indicated by closed and open circles, respectively, to eq 40. (c) Numerical simulation of SPR curves based on a three-layer Fresnel equation of P-polarization using eqs 15−22 and 35 with experimental values in Table 1. (d) Numerical simulation of SPR curves including the spectral broadening of the light source in the SPR curves in part c in order to agree more closely with experimental SPR curves in part a.

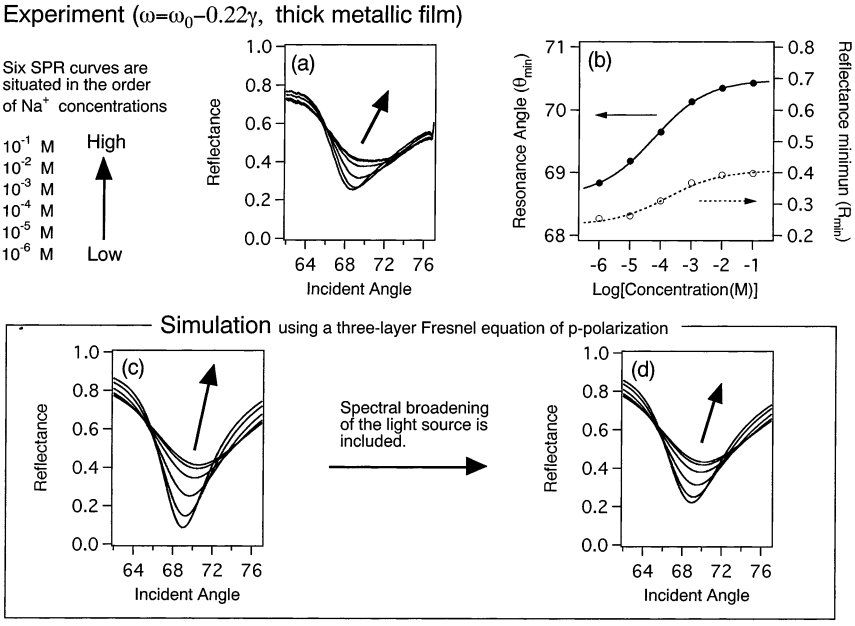

Figure 6. SPR curve response of the SPR sodium ion sensor with a thick metallic thickness of 50 nm under an excitation condition of $\omega = \omega_0 - 0.22\gamma$, where ω, ω_0, and γ are the excitation frequency, the absorption maximum frequency, and the absorption damping frequency. (a) Experimental SPR curves that respond to sodium ion concentrations from 10^{-6} to 10^{-1} M. (b) Dependence of the resonance angle and the reflectance minimum on the sodium ion concentrations from 10^{-6} to 10^{-1} M. (c) Numerical simulation of SPR curves based on a three-layer Fresnel equation of P-polarization under the excitation condition of $\omega = \omega_0 - 0.22\gamma$. (d) Numerical simulation of SPR curves including the spectral broadening of the light source in the SPR curves in part c.

between Figures 5 and 6 enables us to understand the effect of the excitation frequency, or wavelength, of a light source on the absorption-based SPR sensors. In both the cases of $\omega = \omega_0 - 0.05\gamma$ in Figure 5 and $\omega = \omega_0 - 0.22\gamma$ in Figure 6, sodium ion concentrations of 10^{-6}−10^{-1} M were successfully observed by means of the resonance angle as well as the minimum reflectance.

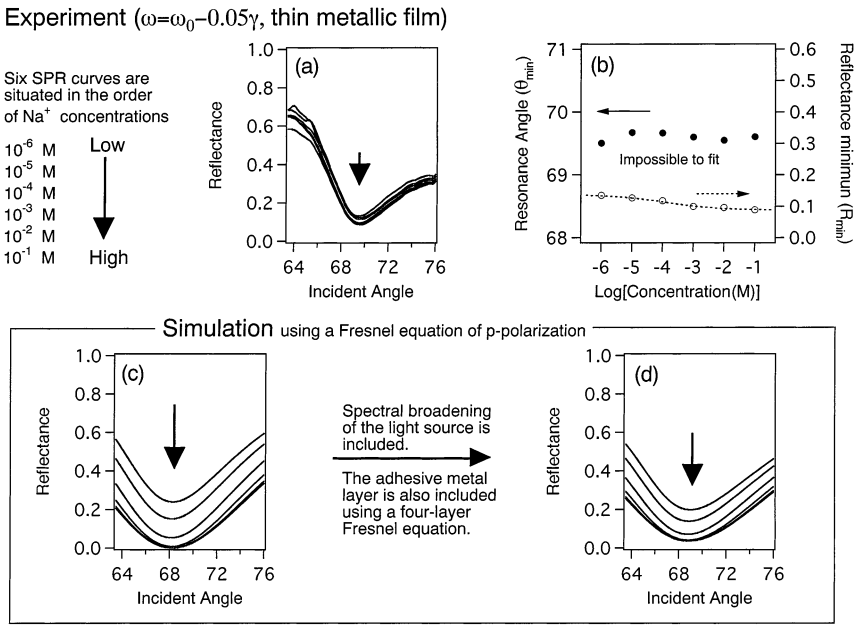

Figure 7. SPR curve response of the SPR sodium ion sensor with a thin metallic thickness of 28 nm under the same excitation condition of $\omega = \omega_0 - 0.05\gamma$ as in Figure 5. (a) Experimental SPR curves that respond to sodium ion concentrations from 10^{-6} to 10^{-1} M. (b) Dependence of the reflectance minimum on the sodium ion concentrations from 10^{-6} to 10^{-1} M. (c) Numerical simulation of SPR curves based on a three-layer Fresnel equation of P-polarization under the excitation condition of $\omega = \omega_0 - 0.05\gamma$. (d) Numerical simulation of SPR curves based on a four-layer Fresnel equation of P-polarization that includes two artifacts in the SPR curves in part c: one is the spectral broadening of the light source, while the other is the adhesive metallic layer between the prism and the metal layer.

When the sodium ion concentrations changed from 10^{-6} to 10^{-1} M, the total change in the resonance angle and the minimum reflectance is 1.1° and 0.16 reflectance unit in Figure 5b and 1.6° and 0.14 reflectance unit in Figure 6b. Interestingly, in the resonance angle diagnosis, the sensitivity of detecting sodium ion concentrations was enhanced by a factor of ~1.5 by changing the excitation frequency from $\omega = \omega_0 - 0.05\gamma$ in Figure 5 to $\omega = \omega_0 - 0.22\gamma$ in Figure 6. According to our previous theoretical article,[3] the rate of increase in the resonance angle with increasing absorption in the sensing layer is zero at $\omega = \omega_0$ but becomes maximum at $\omega = \omega_0 - \gamma/2$. This theoretical description can qualitatively explain the experimental behavior of the resonance angle in the absorption-based SPR ion sensor. In the quantitative considerations in Figure 5, however, the experimental rate of increase in the resonance angle at $\omega = \omega_0 - 0.05\gamma$ was much larger than the theoretically expected value that is close to zero at $\omega = \omega_0$. This can be attributed to the limits of our model in assuming that the absorption frequency remains the same, although it experimentally shifted to a lower frequency with an increasing sodium ion concentration. Figures 5c and 6c show that the simple numerical simulation using the three-layer Fresnel equation is very useful for predicting and understanding qualitative behavior of the absorption-based SPR ion sensor. The numerical simulations were done using eqs 15−22 and 35 with the experimental values in Table 1. Also, the metallic thickness of 50 nm was used for the simulation. To improve the agreement between experimental results and numerical simulations, artificial factors should be included in the numerical simulation such as spectral broadening of the light source, the adhesive metal layer, angular resolution of the SPR instrument, shift in absorption maximum frequency with an increasing sodium ion concentration, and so on. As shown in Figures 5d and 6d, the numerical simulations including one artifact of the spectral broadening of the light source agree more closely with the experimental results. Part d of Figures 5 and 6 agrees much more closely with the experimental SPR curves in part a than part c. This suggests that the spectral broadening of the light source provides a smoothing effect to the SPR curve, resulting in decreasing the sensitivity in the reflectance minimum diagnosis.

On the other hand, a comparison between Figures 5 and 7 enables us to understand the effect of the metallic thickness on the absorption-based SPR sensors because the SPR curves in Figures 5a and 7a were observed with metallic thicknesses of 50 and 28 nm, respectively, under the same excitation condition. The great difference in the SPR curve behavior between Figures 5a and 7a lies in the direction of a change in the minimum reflectance: with increasing sodium concentration, the minimum reflectance increases and decreases in the thick and thin metallic films, respectively. This opposite behavior of the absorption-based SPR curve seems strange at first sight but was adequately predicted in our previous theoretical article.[3] It described that the minimum reflectance simply increases in a thick metallic film with increasing absorption, while it first decreases and then increases in a thin metallic film. In our case, the minimum reflectance simply decreased because the absorption did not increase very much as the minimum reflectance increased after it decreased. In Figure 7b, the reflectance minimum data were successfully fitted to the S-type equation in eq 40, but the resonance angle data could not be fitted because the SPR curves did not change very much as to permit observing changes in the resonance angle. Figure 7c shows a simple numerical simulation of SPR curves using the three-layer Fresnel equation of P-polarization. From the numerical simulation in Figure 7c, we understood that the metallic thickness was critical for the whole SPR curve behavior toward sodium ion concentra-

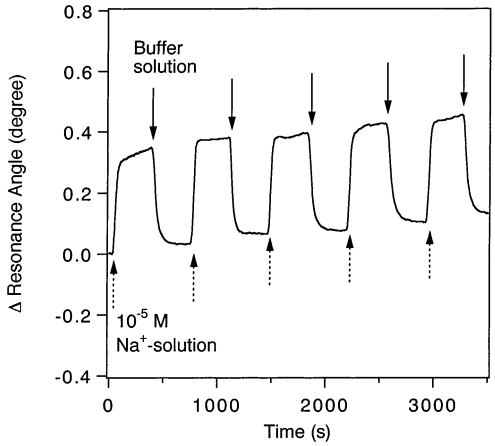

Figure 8. Temporal response of the SPR sodium ion sensor to a repetitive flow of the buffer solution and 10^{-5} M sodium ion solution. The resonance angle shift was monitored in a computer-assisted real-time measurement. Solid and broken line arrows show the time when the buffer and sodium ion solutions, respectively, began to flow.

tions from 10^{-6} to 10^{-1} M. In the numerical simulation using 28-nm metallic thickness in Figure 7c, SPR curves behave as the minimum reflectance simply decreases with increasing sodium ion concentrations. By contrast, in a simulation using a 30-nm metallic thickness, SPR curves behave as the minimum reflectance first decreases and then increases with increasing sodium ion concentrations. Also, the range of the minimum reflectance simulated using 25-nm metallic thickness is 1.3 times wider than that using 28-nm metallic thickness in Figure 7c, though both the SPR curves simulated using 25- and 28-nm metallic thickness behave the same. In Figure 7d, the numerical simulation was improved by including two artifacts of the spectral broadening of the light source and the adhesive metal layer between the prism and the metallic layer. In the improved simulation, we used a four-layer Fresnel equation of P-polarization with a 3-nm adhesive metallic thickness, and its dielectric constant of $-4.01+13.3i$ was referred to the optical properties in Ti,[28] where i is an imaginary number of units. From the numerical simulation in Figure 7d, we understood that the adhesive metallic layer reduces the response range of the minimum reflectance in the SPR curve toward sodium ion concentrations from 10^{-6} to 10^{-1} M. These discussions of the experimental data in Figure 7a demonstrate the validity of the classification of absorption-based SPR curves in Figure 1, though the experimental data are unfortunately not practical for sodium ion sensing.

A Temporal Response of the Absorption-Based SPR Ion Sensor. A real-time measurement of the absorption-based SPR ion sensor was performed under the same conditions as in Figure 7. Investigation of the temporal behavior of the SPR ion sensor is important for accurate determination of ion concentrations. Also, the response time of the SPR ion sensor will be fundamental information for constructing a multichannel SPR sensor that simultaneously detects ions as well as biopolymers such as DNAs and proteins. Figure 8 shows preliminary data on the temporal response of the SPR sodium ion sensor to a repetitive flow of the buffer solution and 10^{-5} M sodium ion solution. The response reflected the sodium ion concentration in the flow. The response time is ~60 s. The drift toward higher angles is probably attributed to the contracting behavior of the ion optode membrane. This temporal measurement was carried out under a limited condition in which the resonance angle was determined by the quadratic fit of the P-polarized angular spectrum in data processing of the SPR sensor system. Much more detailed investigations will be carried out after improvements in the data processing.

Other Important Comments on the Absorption-Based SPR Ion Sensor. When the SPR ion sensor described here is applied for practical use, the sensitivity for ion concentrations can be easily enhanced depending on the preparation of the ion-selective optode membrane. The absorbance of the optode membrane film is proportional to the SPR signal, so that a higher concentration of the pH-sensitive absorption dye in the optode membrane allows for higher sensitivity to ion concentrations. In the case where the concentration of all the chemical components in the plasticized PVC membrane was increased 3 times, the SPR signal in the reflectance diagnosis showed a 3 times greater change. It means that the sensitivity for ion concentrations was improved 3 times.

In the absorption-based SPR ion sensor, it is important for the operating principle that the background dielectric constant of the sensing layer, ϵ_s^∞, in eq 35 is constant relative to ion concentrations of interest. Close fits of the SPR data to the S-type curve in part b of Figures 5−7 indicate that ϵ_s^∞ is constant relative to sodium ion concentrations from 10^{-6} to 10^{-1} M. In part a of Figures 5−7, we did not show SPR curves for the buffer solution, i.e., a sodium ion concentration of 0 M, which was far from what is experimentally expected from SPR curves for sodium ion concentrations from 10^{-6} to 10^{-1} M. In Figure 8, the larger drift was observed in contact with the buffer solution than with the sodium solution. These experimental results suggest that ϵ_s^∞ changes in contact with the buffer solution. Much more detailed investigations are required for the precise determination of ion concentrations.

CONCLUSIONS

According to the concept of the absorption-based SPR sensor, we have developed an SPR sodium ion sensor in a Kretchmann configuration using a sodium ion-selective optode membrane film of ~1-μm thickness covered with a gold metallic film on the prism. The sodium ion optode was composed of plasticized PVC including a neutral sodium ionophore (DD16C5), a pH-sensitive cationic dye (KD-M11), and an anionic additive (TFPB). Its absorption intensity changed with increasing sodium ion concentrations according to the ion-pair/ion-exchange principle. The somewhat complicated behavior of the SPR curve relative to the sodium ion concentrations from 10^{-6} to 10^{-1} M has been accurately observed as being predicted by the absorption-based SPR principle summarized in Figure 1. The sodium ion concentrations have been successfully determined not only by the resonance angle diagnosis but also by the minimum reflectance one. It is noted that SPR signals in the resonance angle diagnosis have been enhanced by a factor of 1.5 when the excitation condition changes from a near-resonant excitation condition, $\omega = \omega_0 - 0.05\gamma$, to an off-resonant one, $\omega = \omega_0 - 0.22\gamma$. We have further investigated the complicated behavior of the SPR curve in an SPR sodium ion sensor using numerical simulations based on a three-layer Fresnel equation of P-polarization including experimental optical constants,

(28) *Handbook of Chemistry and Physics*, 77th ed.; Lide, D. R., Ed.; CRC Press: Boca Raton, FL, 1997.

resulting in close agreement of the SPR curve behavior between the experiments and the simulations. The formula for numerically simulating the SPR curve behavior of the SPR sodium ion sensor is given by eqs 15−22 and 35, where eq 35 is the dielectric constant of the sodium ion optode membrane film including five experimental values. The first is the absorption maximum frequency or wavelength; the second is the absorption damping frequency calculated from the full-width wavelength at half-maximum of the absorption spectrum; the third is the absorbance at the absorption maximum frequency; the fourth is the thickness of the ion optode membrane film when the absorbance is measured; and the fifth is the background dielectric constant of the ion optode membrane given as the square of the refractive index. Also, the numerical simulations including spectral broadening of the light source agree more closely with the experimental results than those not including it. The cooperative combination of the concept and the practical theory of the absorption-based SPR sensor has successfully allowed development of the SPR ion sensor, which was very difficult based on the conventional SPR principle in which only changes in the usual refractive index are monitored. Our demonstration of the absorption-based SPR sensor applied to ion sensing will accelerate the introduction of conventional chemical analysis based on optical absorption into the SPR method.

ACKNOWLEDGMENT

We thank Drs. O. Niwa and Y. Iwasaki of the NTT Microsystem Integration Laboratories, Mr. T. Tobita of the NTT Advanced Technology Corp., and Mr. H. Hashimoto of the Airport Environment Improvement Foundation for their friendly cooperation in the absorption-based SPR experiments.

Received for review May 14, 2002. Accepted October 8, 2002.

AC0203241